Page 1 of 22. © Royal Aeronautical Society Year
doi: 10.1017/aer.2016.1

An extended invariant approach to laminate failure of fibre-reinforced polymer structures

G. Corrado
giuseppe.corrado@airbus.com

Airbus Defence and Space GmbH
Stress Methods and Optimisation
Manching
Germany

Faculty of Engineering, University of Porto
Department of Mechanical Engineering
Porto
Portugal

A. Arteiro and A.T. Marques
aarteirto@fe.up.pt

Faculty of Engineering, University of Porto
Department of Mechanical Engineering
Porto
Portugal

J. Reinoso

School of Engineering, University of Seville
Group of Elasticity and Strength of Materials
Seville
Spain

F. Daoud and F. Glock

Airbus Defence and Space GmbH
Stress Methods and Optimisation
Manching
Germany

Received DD MM YYYY; revised DD MM YYYY; accepted DD MM YYYY.

ABSTRACT

This paper presents the development of omni-failure envelopes for advanced composite materials based on phenomenological failure criteria in order to predict failure of composite laminates under general three-dimensional (3D) stress states. Phenomenological failure criteria based on invariant structural tensors are extended to address failure events in multidirectional laminates using the "omni strain failure envelope" concept. This concept enables the generation of safe predictions of first-ply failure (FPF) and last-ply failure (LPF) of composite laminates, which can be particularly useful as a design tool by providing reliable and fast indications suitable for conceptual and preliminary design of composite structures. The proposed extended omni strain failure envelopes allow not only identification of the controlling plies for FPF and LPF, but also the controlling FPF modes and FPF/LPF surfaces under general 3D stress states. These surfaces can be obtained using only the material properties extracted from the UD material, and can predict membrane FPF or LPF of any laminate, independently of lay-up or stacking sequence, while considering the effect of out-of-plane stresses. The predictions of the LPF envelopes and surfaces are compared with experimental data on multidirectional laminates from the first and second World-Wide Failure Exercise (WWFE), showing a satisfactory agreement.

Keywords: Failure Criteria; Laminates; Polymer-matrix composites; Strength; Analytical modelling; Laminate mechanics

NOMENCLATURE

a	Preferred direction
A	Structural tensor
CFRP	Carbon fibre reinforced polymer
E_i	Elastic modulus in the i-direction
F_{12}^*	Interaction term from the Tsai-Wu failure theory
FI_{F}	Failure index for fibre tensile failure onset
FI_{K}	Failure index for fibre kinking
FI_{M}	Failure index for matrix failure onset
FPF	First-ply failure
FRP	Fibre reinforced polymer
G_{12}, G_{23}	In-plane and transverse shear moduli
GFRP	Glass fibre reinforced polymer
I_i	ith invariant of the stress tensor
LPF	Last-ply failure
S_L, S_T	In-plane and transverse shear strength
UD	Unidirectional
WWFE	World wide failure exercise
X_c	Compressive strength in the fibre direction
X_t	Tensile strength in the fibre direction
Y_{bc}	Transverse biaxial compressive strength
Y_{bt}	Transverse biaxial tensile strength
Y_c	Compressive strength in the transverse direction
Y_t	Tensile strength in the transverse direction

Greek Symbol

α_{ij}	Failure parameters
$\boldsymbol{\varepsilon}$	Strain tensor
$\varepsilon_{\mathrm{Xc}}, \varepsilon_{\mathrm{Xt}}$	Compressive and tensile strain-to-failure
ν_{12}, ν_{23}	In-plane and transverse Poisson's ratio
$\boldsymbol{\sigma}$	Stress tensor
$\boldsymbol{\sigma}^p$	Crack inducing components of the stress tensor
$\boldsymbol{\sigma}^r$	Reaction components of the stress tensor
φ	Kinking angle
φ_c	Kinking angle under pure longitudinal compression
χ	Micro-mechanical parameter
ψ	Angle of the kinking plane

1.0 BACKGROUND

Failure criteria are defined to set the limit values in stress (or strain) space beyond which the material experiences a certain level of structural degradation due to inelastic effects from different signature. Therefore, they provide a robust tool for predicting the loss of integrity that could lead to the structural collapse of the studied component[1]. For instance, failure criteria are crucial at early design stages, especially when providing failure envelopes in the stress (or strain) space from relatively simple experimental data. This enables the calculation of safety factors of composite structures subjected to complex loading and boundary conditions.

Over the last five decades, the development of failure criteria for composite materials has found continuous efforts worldwide that has led to the proposal of several failure criteria. As a direct consequence, many reviews of failure theories were published so far. One of the proposed classifications of these theories was made by distinguishing theories that do not account for different failure modes, denoted as *non-phenomenological failure criteria*, and failure theories that are able to identify the different failure modes, denoted as *phenomenological failure criteria*[2,3]. The first group comprises criteria in which a failure envelope is defined by using a mathematical expression, usually a polynomial form, which predicts failure by interpolating between a few experimental points. No attempt is made in order to predict which failure mode is taking place, and the criterion itself does not integrate any physical consideration. Tsai-Wu and Tsai-Hill are two common examples of non-phenomenological failure theories. Failure criteria of the second family predict failure based on physical considerations for the specific failure modes.

The need for failure criteria based on failure mechanisms dates back to 1973, when Hashin used his experimental studies to establish two different formulations in order to identify fibre failure and matrix failure mechanisms in a independent manner. According to some reviews, however, the first model distinguishing failure modes was proposed by Puck in 1969[4], although his theory has found more resonance in the composites community with the work published in 1998[5]. Among the available phenomenological failure criteria, Hashin, Puck and LaRC failure theories can be highlighted[6,7,8].

More recently, a new set of failure criteria based on structural invariants was proposed, commonly referred to as 3D invariant-based failure criteria[9], which have provided satisfactory agreements with respect to experimental data and therefore they can be considered as potential predictive tools for composite designs in engineering practice.

1.1 3D invariant-based failure criteria

Among the most recent phenomenological failure criteria proposed for fibre-reinforced polymers (FRPs), a set of advanced phenomenological failure theories was selected for the present work due to its unique 3D character. These new criteria are based on the transversely isotropic yield function developed by Vogler et al.[10]. They have an invariant quadratic formulation involving structural tensors that accounts for the preferred material directions of the anisotropic material. With this formulation, anisotropy is derived using structural tensors and not symmetry conditions based on a reference coordinate system. These advantageous features enable a simpler and elegant description of failure of composites[9].

The invariant-based failure criterion for transverse failure of unidirectional composites is given as:

$$FI_{\mathrm{M}} = \begin{cases} \alpha_1 I_1 + \alpha_2 I_2 + \alpha_3^t I_3 + \alpha_{32}^t I_3^2 & \text{for} \quad I_3 > 0 \\ \alpha_1 I_1 + \alpha_2 I_2 + \alpha_3^c I_3 + \alpha_{32}^c I_3^2 & \text{for} \quad I_3 \leq 0 \end{cases} \tag{1}$$

where the stress invariants (I_1, I_2, I_3) for matrix failure are defined as:

$$I_1 = \frac{1}{4}\sigma_{22}^2 - \frac{1}{2}\sigma_{22}\sigma_{33} + \frac{1}{4}\sigma_{33}^2 + \sigma_{23}^2, \qquad I_2 = \sigma_{12}^2 + \sigma_{13}^2, \qquad I_3 = \sigma_{22} + \sigma_{33} \tag{2}$$

and the failure parameters α are given by:

$$\alpha_1 = \frac{1}{S_T^2}, \quad \alpha_{32}^t = \frac{1 - \dfrac{Y_t}{2Y_{bt}} - \alpha_1 \dfrac{Y_t^2}{4}}{Y_t^2 - 2Y_{bt}Y_t}, \quad \alpha_3^t = \frac{1}{2Y_{bt}} - 2\alpha_{32}^t Y_{bt},$$

$$\alpha_2 = \frac{1}{S_L^2}, \quad \alpha_{32}^c = \frac{1 - \dfrac{Y_c}{2Y_{bc}} - \alpha_1 \dfrac{Y_c^2}{4}}{Y_c^2 - 2Y_{bc}Y_c}, \quad \alpha_3^c = \frac{1}{2Y_{bc}} - 2\alpha_{32}^c Y_{bc}. \tag{3}$$

S_T and S_L are respectively the transverse and in-plane shear strengths, Y_c and Y_{bc} are respectively the transverse uniaxial and biaxial compressive strengths, and Y_t and Y_{bt} are respectively the transverse uniaxial and biaxial tensile strengths. Through the sign of the third invariant I_3 this criterion is able to address failure under biaxial stress states.

Fibre failure under tension is predicted using the non-interactive maximum allowable strain criterion, following the LaRC03 criteria[6]. Since the failure mechanism under longitudinal compression of carbon fibre reinforced polymers (CFRPs) involves mainly the formation of a kink band, resulting from micro-buckled fibres and local matrix cracking, Camanho et al.[9] proposed a 3D kinking model by recalling the invariant-based failure criterion for transverse failure, but in the misalignment frame of the kinked fibres. In fact, by determining the angle of the kinking plane ψ and the kinking angle φ based on the kinematics of fibre kinking, it is possible to formulate the invariant-based failure criterion for kinking failure prediction in the fibres misalignment frame.

Figure 1 shows the kinking plane and the 3 coordinate systems: the initial coordinate system ($1^0 2^0 3^0$), associated with the material axes of the composite, the coordinate system related with the kinking plane ($1^\psi 2^\psi 3^\psi$) and the coordinate system related with the misaligned fibres ($1^\varphi 2^\varphi 3^\varphi$). The invariant-based failure criterion for fibre kinking is formulated in the latter

coordinate system. In a compact form, the failure criteria for fibre failure can be presented in the following way:

$$FI_{\mathrm{F}} = \frac{\varepsilon_1}{\varepsilon_{\mathrm{Xt}}} \quad \text{for} \quad \sigma_{11} \geq 0 \tag{4}$$

$$FI_{\mathrm{K}} = \begin{cases} \alpha_1 I_1 + \alpha_2 I_2 + \alpha_3^t I_3 + \alpha_{32}^t I_3^2 & \text{for} \quad \sigma_{11} < 0 \quad \text{and} \quad \mathrm{I}_3 > 0 \\ \alpha_1 I_1 + \alpha_2 I_2 + \alpha_3^c I_3 + \alpha_{32}^c I_3^2 & \text{for} \quad \sigma_{11} < 0 \quad \text{and} \quad \mathrm{I}_3 \leq 0 \end{cases} \tag{5}$$

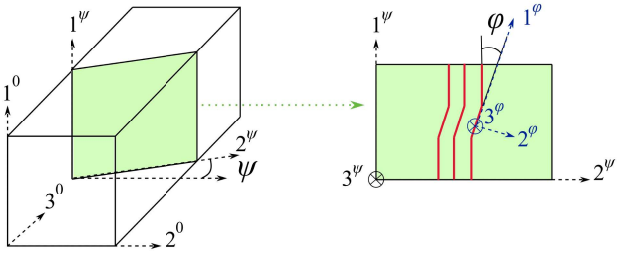

Fig. 1. 3D kinking model with the definition of the kinking angle φ and the angle of the kinking plane ψ.

where $\varepsilon_{\mathrm{Xt}}$ is the ultimate tensile strain. In order to formulate the stress tensors, the definition of the preferred direction $\mathbf{a}$, corresponding to the fibre direction in the misalignment frame, is required. This direction is obtained by performing two transformations of coordinate system to get to the initial ($1^0 2^0 3^0$) system:

$$\mathbf{a}^{(0)} = \begin{bmatrix} \cos\varphi \\ \cos\psi \sin\varphi \\ \sin\psi \sin\varphi \end{bmatrix} \tag{6}$$

The structural tensor $\mathbf{A}$ that represents the transversely isotropic properties of the material is defined as:

$$\mathbf{A} = \mathbf{a} \otimes \mathbf{a} \tag{7}$$

The stress invariants needed for the coordinate system-free formulation of the invariant-based criterion can be now formulated as a function of the preferred direction $\mathbf{a}$, the structural tensor $\mathbf{A}$, and the stress tensor $\boldsymbol{\sigma}$ based on its crack inducing components $\boldsymbol{\sigma}^p$ and the reaction components $\boldsymbol{\sigma}^r$:

$$I_1 = \frac{1}{2}\mathrm{tr}\,(\boldsymbol{\sigma}^p)^2 - \mathbf{a}\,(\boldsymbol{\sigma}^p)^2\,\mathbf{a}, \qquad I_2 = \mathbf{a}\,(\boldsymbol{\sigma}^p)^2\,\mathbf{a}, \qquad I_3 = \mathrm{tr}\,\boldsymbol{\sigma} - \mathbf{a}\boldsymbol{\sigma}\mathbf{a} \tag{8}$$

with:

$$\boldsymbol{\sigma}^r = \frac{1}{2}(\mathrm{tr}\,\boldsymbol{\sigma} - \mathbf{a}\boldsymbol{\sigma}\mathbf{a})\mathbf{1} - \frac{1}{2}(\mathrm{tr}\,\boldsymbol{\sigma} - 3\mathbf{a}\boldsymbol{\sigma}\mathbf{a})\mathbf{A}, \qquad \boldsymbol{\sigma}^p = \boldsymbol{\sigma} - \boldsymbol{\sigma}^r \tag{9}$$

The angle of the kinking plane ψ is determined using a pragmatic approach considering the shear stresses acting on the transversely isotropic plane (if these components are not zero)[7,8]:

$$\psi = \arctan\left(\frac{\sigma_{13}}{\sigma_{12}}\right) \tag{10}$$

Otherwise the angle of the kinking plane is calculated by the maximum principal stress that acts on the transversely isotropic plane:

$$\psi = \frac{1}{2}\arctan\left(\frac{2\sigma_{23}}{\sigma_{22}-\sigma_{33}}\right) \tag{11}$$

The kinking angle φ is determined as proposed by Catalanotti et al.[8], in which a micro-mechanical parameter χ is introduced to account for the micro-structural effects that control the development of fibre kinking:

$$\chi = -\frac{\sin 2\varphi_c X_c}{2\,\varphi_c} \tag{12}$$

where φ_c is the kinking angle under pure longitudinal compression and X_c is the longitudinal compressive strength. As suggested by the authors of this formulation[8], the kinking angle φ can be found imposing the stress equilibrium in the frame of the kink band and solving the nonlinear equation, applying the bisection method. The determination of the kinking angle φ_c is made by solving the invariant-based failure criteria for a pure longitudinal compressive stress state and knowing that, at failure, the criterion in Eq. (5) yields 1, with $\sigma_{11} = X_c$ and $\varphi = \varphi_c$. Solving for φ_c:

$$\begin{aligned}\varphi_c = \frac{1}{2}\arccos\Big\{\Big[4\sqrt{\alpha_1 - 4\alpha_2 + \alpha_2^2 X_c^2 + \left(\alpha_3^c\right)^2 + 2\alpha_2\alpha_3^c X_c + 4\alpha_{32}^c}\; + \\ + \left(\alpha_1 + 4\alpha_{32}^c\right)X_c + 4\alpha_3^c\Big]\cdot\Big[\left(\alpha_1 - 4\alpha_2 + 4\alpha_{32}^c\right)X_c\Big]^{-1}\Big\}\end{aligned} \tag{13}$$

It is important to emphasize that this set of invariant-based failure criteria is completely formulated in a 3D setting, unlike other phenomenological failure criteria that were initially formulated in a 2D setting and then extended to the 3D case. Additional details, such as a pragmatic approach for the determination of the fracture plane and the definition of the *in situ* properties, can be found in Ref.[11].

Several validation studies of these criteria were performed, comparing the predictions with experimental data obtained for different material systems under various scenarios of multiaxial loading. In particular, these criteria are capable of predicting the evolution of the shear stress with hydrostatic pressure, which no previous failure criteria have taken into account. Furthermore, a good agreement between the failure envelopes predicted by computational micro-mechanics and the 3D invariant-based failure criteria were reported. While Hashin's criteria show an open failure envelope for the biaxial transverse compression quadrant, thus making it unsuitable for representing the fracture of composites subjected to high hydrostatic stresses, the 3D invariant-based failure criteria accurately represented the failure envelopes under both tension-tension and compression-compression biaxial stress states[9].

The validation studies performed by Camanho et al.[9] include experimental results from open literature (such as the first WWFE, where only biaxial tests are discussed) and additional data obtained using computational micro-mechanics to complement the available database, without requiring very expensive test setups.

To further challenge the 3D invariant-based theory in the prediction of failure under triaxial stress states, experimental results from the WWFE-II[12] are considered here. Figs. 2-5 show the correlation of the predicted envelopes against experimental results from the WWFE-II for UD S-glass/epoxy, carbon/epoxy, E-glass/MY750 and T300/PR319 respectively. The

predictions of the 3D invariant-based theory are also compared with those obtained using the Tsai-Wu failure surface for the same test cases.

The mechanical properties of the tested materials can be found in Ref.[12]; however, since biaxial strengths are not provided, they have been assumed after assessing their effect on the predicted envelopes. Furthermore, the transverse shear strength S_T is assumed equal to the transverse tensile strength Y_T, following the observations from Refs.[13,5]. The influence of Y_{bc} on the strength predictions of the invariant-based theory was investigated for each case and it is included in the respective figures. With the same scope, the effect of the interaction term F_{12}^* from the Tsai-Wu theory was studied and it is also shown. All the test cases highlight that the 3D invariant-based theory offers a remarkable flexibility in fitting complex results with Y_{bc}, while the interaction term from Tsai-Wu cannot always help the correlation with experimental data. Indeed, except for the third case (Fig. 4) where the strength predictions are very sensitive to the value of the interaction term, a non-zero F_{12}^* results in open envelopes for the first 2 cases (Figs. 2-3) and in almost coincident predictions in the last case (Fig. 5).

In general, the failure predictions based on Tsai-Wu criterion exhibited some deviations with respect to the experimental data when dealing with triaxial failure stress states. In spite of the large scatter of the test results and the complexity of the considered test cases, a generally good fit can be observed when using the 3D invariant-based failure criteria.

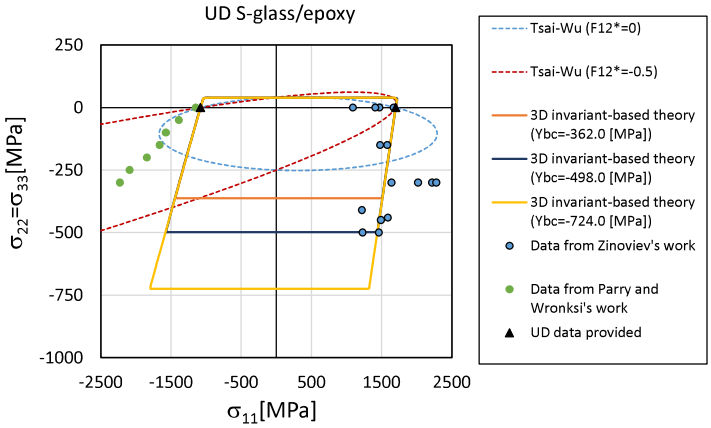

Fig. 2. Triaxial failure stress states: σ_{22}=σ_{33} vs. longitudinal stress σ_{11} for a UD S-glass/epoxy.

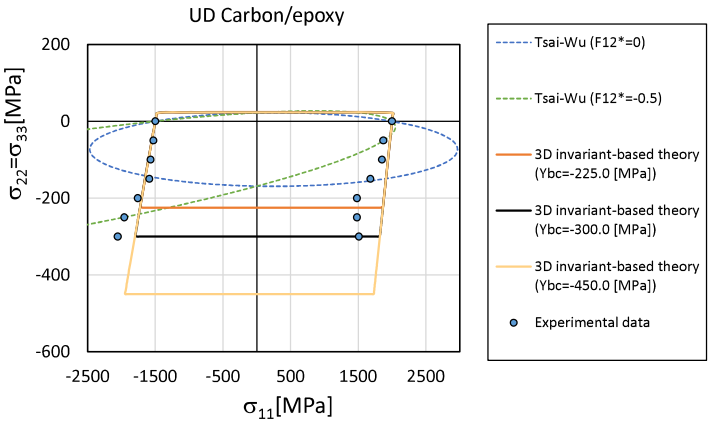

Fig. 3. Triaxial failure stress states: σ_{22}=σ_{33} vs. longitudinal stress σ_{11} for a UD carbon/epoxy cube.

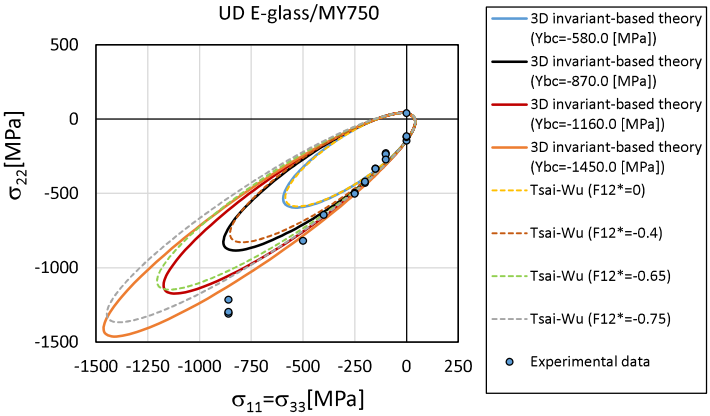

Fig. 4. Triaxial failure stress states: σ_{22} vs. longitudinal stress σ_{11}=σ_{33} for a UD E-glass/MY750 epoxy.

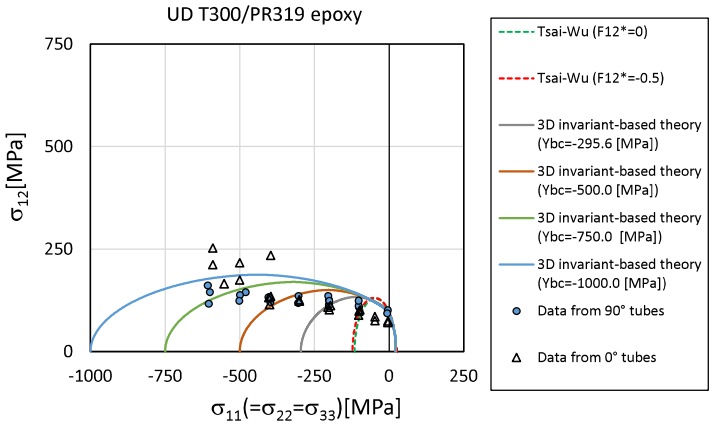

Fig. 5. Triaxial failure stress states: shear stress σ_{12} vs. hydrostatic pressure (σ_{11}=σ_{22}=σ_{33}) for a UD T300/PR319 epoxy.

1.2 Omni strain failure envelopes

The previous criteria for the prediction of intralaminar failure can be implemented to perform ply-by-ply failure analysis with the aim of aiding the design of composite laminates. However, when the number of layers in the laminate is large or for large-scale simulations of composite structures, the computational cost of ply-by-ply or layerwise representations becomes huge, making the meso-scale analysis unsuitable for the mentioned applications. For these reasons, alternative approaches at the macro-scale, i.e., laminate level, must be considered in the numerical failure predictions[14,15].

In this framework, to meet the industrial need for fast and practical tools at an early design stage and optimization of large-scale composite structures (such as fuselage, wings or empennage), simplified and reliable approaches for the prediction of last-ply failure of any composite laminates have been developed. Following this idea, Tsai and Melo proposed a novel invariant approach for the description of the mechanical response of composite laminates[16]. They introduced the "omni strain" failure envelope, also denoted as minimum FPF (first-ply-failure) envelope, as the inner failure envelope in strain space, obtained by finding the controlling ply that would fail first for unit loading strain vectors from 0 to 2π. Omni strain envelopes can be considered a material property independent of the laminate layup composition, thanks to their capability of describing the failure of any laminate by covering all possible fibre orientations.

Omni strain envelopes are presented in strain space, since the shape of the envelope remains independent of adding other plies. Therefore, only in strain space it is possible to superimpose the failure envelopes for the different ply orientations and compute a laminate failure envelope. Fig. 6 shows the omni strain failure envelopes based on the Tsai-Wu failure criterion for two different materials. It can be noted that, with this approach, all laminate data can be displayed on one graph in strain space, realizing a very concise display of the strength of a given composite material. Furthermore, it is a very practical tool, enabling a fast selection of the stacking sequence according to the required mechanical properties, since it covers all the possible ply orientations.

For the implementation of omni strain FPF envelopes, the use of polynomial tensor-based

failure criteria is interesting, as there are established transformation relations that enable the reformulation of the criteria from stress space to strain space. This transformation relations are described in Ref.[16], where the Tsai-Wu failure criterion is reformulated in strain space:

$$G_{ij}\varepsilon_i\varepsilon_j + G_i\varepsilon_i = 1 \tag{14}$$

where G_{ij} and G_i are the strength parameters in strain space, which can be expressed as a function of the strength parameters in stress space F_{ij} and F_i as follows: $G_{ij} = F_{kl}Q_{ki}Q_{lj}$, $G_j = F_jQ_{ij}$, where Q_{ij} is the in-plane stiffness matrix. However, any failure theory can be applied for the generation of omni FPF envelopes.

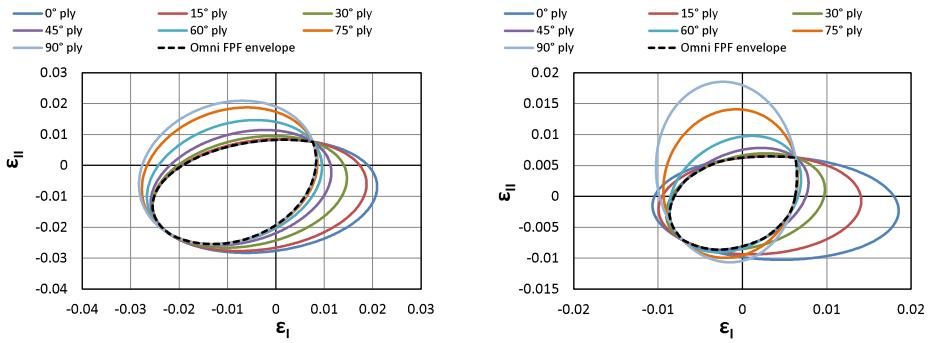

(a) T700/C-Ply 55. (b) IM7/977-3.

Fig. 6. Omni FPF envelopes in principal strain space for T700/C-Ply 55 (a) and IM7/977-3 (b) laminates, according to the Tsai-Wu failure criterion.

Because the omni FPF envelopes represent the most conservative design solution, where all the plies remain undamaged, Tsai and Melo proposed an extended version of this criterion, to define and predict the continued load-carrying capability of any laminate, after damage initiation. They introduced the omni last-ply-failure (LPF) envelope[17], which is an extension of the concept of omni FPF envelope to ultimate failure. The construction of these envelopes follows the same procedure as described before, but with degraded ply properties, based on a matrix degradation factor (E_m^*) and micro-mechanics relations. Moreover, Tsai and Melo observed that, for all CFRP laminates, the inner LPF envelope is controlled by the 0° and 90° plies loaded along the respective fibre direction.

Based on these observations, a further simplification of the failure analysis was performed introducing the unit circle failure envelopes, which can be easily represented by defining the "anchor points" as shown in Fig. 7a. Failure envelopes can be derived for any CFRP if the anchor points are multiplied by the respective tensile and compressive strains-to-failure ε_{Xt} and ε_{Xc}, respectively. Comparing the omni strain LPF envelope and the unit circle failure envelope of the same material, as shown in Fig. 7b, the unit circle envelope is inscribed in the omni LPF envelope. This was also demonstrated by Tsai and Melo for different CFRPs. Although the failure predictions related with this criteria are intentionally conservative, this theory is extremely useful. In particular, the great advantage of using the unit circle failure envelope is that it only requires the strains-to-failure of a 0° coupon measured in tension and in compression instead of complete characterization of the ply properties required by the omni strain LPF envelope.

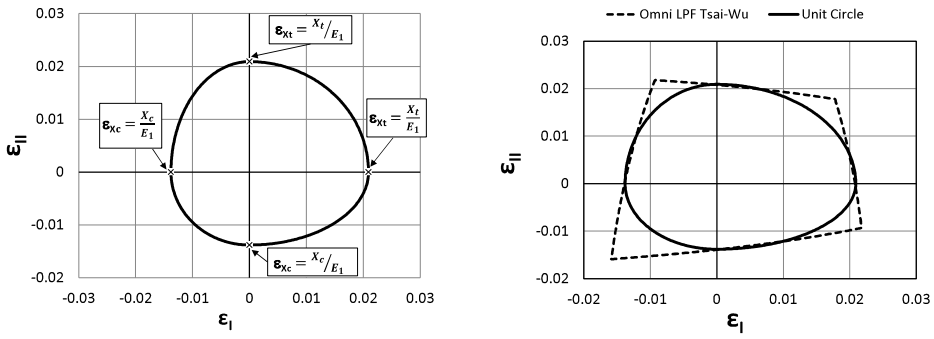

(a) Anchor points. (b) Unit circle and omni LPF envelope.

Fig. 7. (a) Definition of anchor points for a unit circle failure envelope in principal strain space; (b) unit circle (solid line) and omni strain LPF (dashed line) envelopes for T700/C-Ply 55 carbon/epoxy.

Since the "omni failure" concept was proposed using the Tsai-Wu failure criterion, the resulting method was able to highlight the controlling plies, but not the critical failure modes. Moreover, the Tsai-Wu criterion is mostly used for plane stress conditions, inhibiting the prediction of failure under complex triaxial stress states (as observed in mechanically fastened connections, or in thick composite structures, such as at the wing-to-fuselage assembly wingbox or at the bulkhead-stringer run-outs connection). Hence, to extend the applicability of the omni strain failure envelopes concept, the invariant-based failure theory is proposed for generation of phenomenological 3D omni strain failure surfaces, enabling the application of omni criteria in sizing of composite structures subjected not only to plane stress conditions, but also general 3D stress states.

2.0 EXTENDED OMNI STRAIN FAILURE ENVELOPES

Exploiting the fully 3D description of failure provided by the invariant-based theory outlined in Section 1.1, omni strain failure envelopes can be extended by finding the controlling plies in the 3D principal strain space. Indeed, with this extension, the resulting design space can predict laminate failure under complex 3D stress states and address, for instance, the design of bolted joints or thick composite laminates, where through-thickness stress states cannot be neglected. Furthermore, in this case, the envelopes allow the identification of the critical failure modes for each controlling ply, which cannot be investigated with the Tsai-Wu based omni strain envelopes.

An example of omni FPF envelope, obtained using the invariant-based failure model for IM7/8552, is shown in Fig. 8. On the left-hand side, several ply failure envelopes are represented with different colors, from which the omni strain FPF envelope with a black dotted line can be obtained. Fig. 8b provides a detailed view of the omni FPF envelope only, where the failure loci are represented using different markers in order to identify the critical failure modes for each controlling ply ([0], [90], [75] and [15]). In this way, it is possible to identify fibre failure as the most prominent FPF mode shaping the omni FPF envelope of IM7/8552.

Furthermore, when fibre kinking occurs, the kinking angle φ and the angle of the kinking

plane ψ, computed as described in the failure model, can be recorded and added to the plot. To give an example, Fig. 9 shows the evolution of the kinking angle on the omni FPF envelope for IM7/8552. It can be observed that the predicted kinking angle in the minimum FPF envelope ranges, in absolute values, from 0° to 8.6°, reaching the maximum absolute value in the compression-compression quadrant, under the highest value of applied biaxial compressive strain.

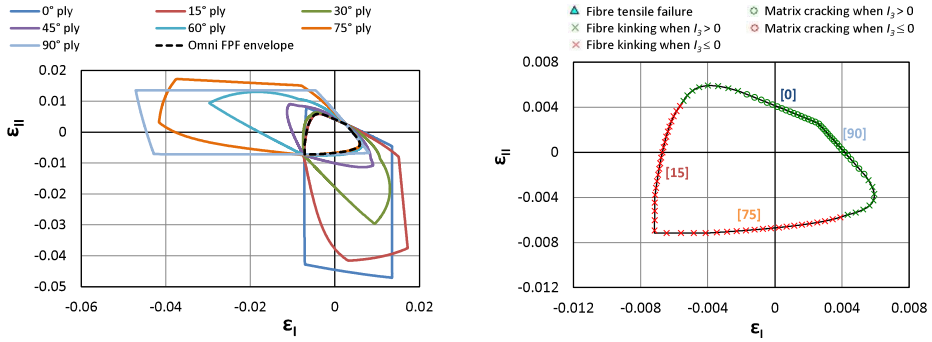

(a) Omni FPF envelope. (b) Controlling plies and failure modes.

Fig. 8. Omni FPF envelope in strain space for IM7/8552, according to the 3D invariant-based failure criteria, with a detailed view on the critical failure modes.

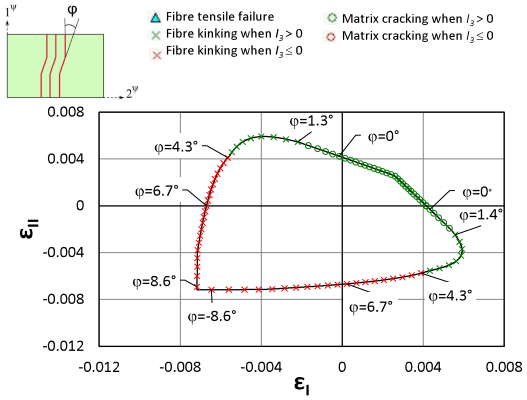

Fig. 9. Detailed view on the values of kinking angle φ on the omni FPF envelope in principal strain space for IM7/8552, according to the 3D invariant-based failure model.

Following Ref.[17], the degraded ply properties of IM7/8552 are computing using micromechanics relations and a matrix degradation factor equal to 0.15. The omni LPF envelope can be finally generated, as shown in Fig. 10. In a similar illustrative scheme as for the omni FPF envelope, the controlling plies and the critical failure modes are highlighted in the figure. In particular, Fig. 10b shows that LPF is dominated by fibre failure, in agreement with the observations of Tsai and Melo[17].

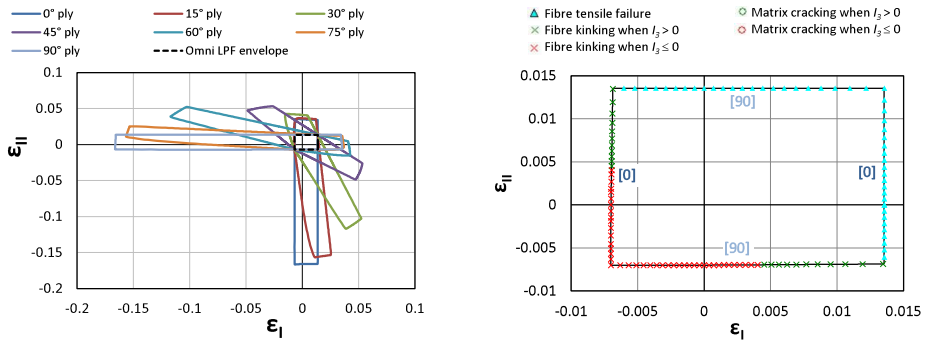

(a) Omni LPF envelope.

(b) Identification of controlling plies and failure modes.

Fig. 10. Omni LFP envelope in principal strain space for IM7/8552, according to the 3D invariant-based failure criteria, with a detailed view of the controlling plies and critical failure modes.

This invariant-based description of failure can be represented in 3D, as the set of invariant-based failure criteria captures well the effect of the out-of-plane direction. For IM7/8552, the failure surface in stress space is shown in Fig. 11, while the omni FPF and LPF surfaces are represented in Figs. 12a and 12b, respectively. As a remark, these surfaces predict membrane FPF or LPF of any laminate, independently of lay-up or stacking sequence, while considering the effect of out-of-plane stresses, and can be obtained using only the material properties of the UD material required by the failure model. For this reason, this approach can be very effective in guiding the conceptual design of composite structures subjected to any stress state.

It is also important to stress that, for typical CFRP laminates, such as aerospace industry-standard "quad" laminates characterized by different percentage of 0°, ±45° and 90° plies[18], omni LPF and laminate LPF envelopes (the latter obtained from superposing in strain space only the envelopes of the ply orientations contained in the selected laminate) will lead to the same laminate failure predictions. This is justified by the presence of the [0] and [90] plies in these laminates, which will govern LPF according to both approaches. Therefore, for all CFRP quad laminates, the omni LPF envelopes ensure the same degree of conservatism as the laminate LPF envelopes, but without the need to recompute the failure envelope everytime the layup changes. On the other hand, when tackling LPF of angle-ply laminates, omni LPF envelopes will have a certain degree of conservatism that will depend on the ply angles.

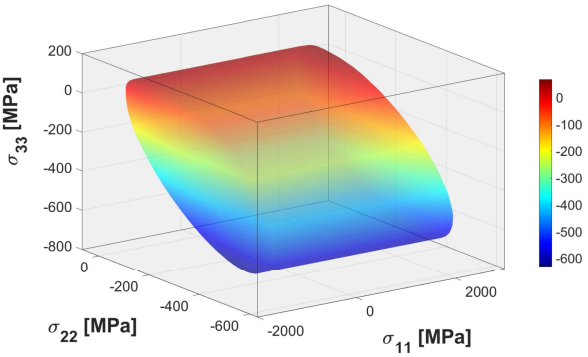

Fig. 11. 3D failure surface in stress space for UD IM7/8552, obtained using the 3D invariant-based failure criteria.

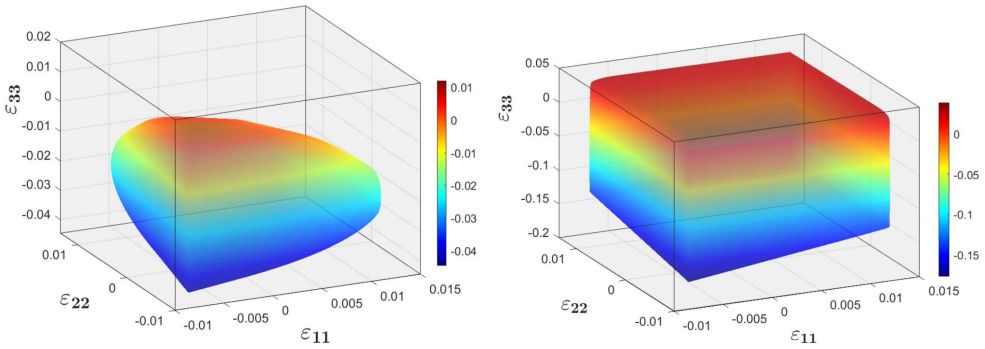

(a) 3D omni strain FPF surface. (b) 3D omni strain LPF surface.

Fig. 12. 3D omni strain FPF (a) and LPF (b) surfaces in strain space for IM7/8552, obtained using the 3D invariant-based failure criteria.

3.0 VALIDATION OF THE EXTENDED OMNI ENVELOPES

In this section, the reliability and the overall performance of these "extended" omni strain LPF envelopes in predicting laminate failure is assessed using experimental data from the first and the second WWFE[12,19,20]. For the validation studies involving biaxial experimental data, omni LPF envelopes are generated using the Tsai-Wu and the 3D invariant-based failure criteria outlined in Section 1.1. For all the considered criteria, the envelopes are calculated using a matrix degradation factor of 0.15, which however lowers the differences in the failure predictions between the different criteria. In fact, when the matrix degradation factor approaches to zero, the predictions of the criteria in 2D become coincident. The degraded elastic properties used for omni LPF envelopes are: $E_2(= E_3)$, G_{12} and ν_{12}. The interaction term F_{12}^* of the Tsai-Wu failure theory is considered equal to -0.5 for all the considered test cases.

The first WWFE provides several test cases including biaxial failure stress envelopes for different laminates. In this validation study, the following laminates have been

considered: AS4/3501-6 [90/±45/0]s, E-glass/LY556/HT907/DY063 [±30/90]s and E-glass/MY750/HY750/DY063 [±55]s. The material properties of their unidirectional plies are provided in Table 1. The additional mechanical properties required for the 3D invariant-based failure theory (Y_{bc}, Y_{bt}) are not provided in the WWFE-I, but they are scaled following the observations from Ref.[10]. Since the experimental data from literature are presented in stress space, laminate stress-strain relations have been used to represent omni LPF envelopes in stress space and compared with the available data.

Table 1
Material properties from WWFE-I[19].

Material	E_1[GPa]	E_2[GPa]	ν_{12}	G_{12}[GPa]	X_t-X_c[MPa]	Y_t-Y_c[MPa]	S_L[MPa]
AS4/3501-6	126.0	11.0	0.28	6.6	1950 - 1480	48 - 200	79
E-glass/LY556	53.48	17.7	0.28	5.83	1140 - 570	35 - 114	72
E-glass/MY750	45.6	16.2	0.28	5.83	1280 - 800	40 - 145	73

Fig. 13 presents the comparison between experimental results and the proposed envelopes for an AS4/3501-6 [90/±45/0]s laminate. On the left-hand side, Fig. 13a shows the omni FPF envelopes obtained with Tsai-Wu and the invariant-based theory, while in Fig. 13b the omni LPF envelopes based on the same criteria and the unit circle predictions are included. The conservatism of the omni FPF approach can be observed when using both theories and, in particular, in the strength predictions in the first and fourth quadrant. This can be explained by the critical failure mode under those stress states, which is matrix cracking for FPF.

Small differences can be observed between the 2 omni LPF envelopes (obtained using the 3D invariant-based failure criteria in black and Tsai-Wu in green solid line), but in general, the predictions obtained with Tsai-Wu and the unit circle envelope are slightly more conservative compared with the invariant-based theory. The correlation between test data and predictions is excellent, except for the third quadrant where the predictions seem to overestimate the laminate strength under biaxial compression. However, those experimental results from Swanson and Colvin cannot be considered 100% reliable, as pointed out also by the organizers of the first WWFE[19], being characterized by a large scatter in the mean axial compressive strength, probably affected by buckling when testing longer specimens. Thus, the predictive capability of the considered approaches cannot be reliably assessed in the compression-compression quadrant.

The correlation between the failure predictions using omni FPF envelopes and experimental data for a [±30/90]s laminate made of E-glass/LY556/HT907/DY063, shown in Fig. 14a, highlights the remarkable conservatism of the approach and the large difference when compared with omni LPF and unit circle envelopes shown in Fig. 14b. The failure predictions obtained with the 2 omni LPF envelopes are almost coincident, while the unit circle is less conservative than the omni LPF envelopes. Unlike CFRPs, fibre failure is not always the critical failure mode for glass-fibre reinforced plastics (GFRPs).

To confirm this observation, Figs. 15 and 16 show the omni LPF envelopes in strain space for the E-glass composites herein (Table 1), highlighting that the controlling plies are not always [0] and [90], and that matrix failure defines almost half of the envelopes for these materials. This confirms that the assumption of fibre failure for LPF is only true when studying

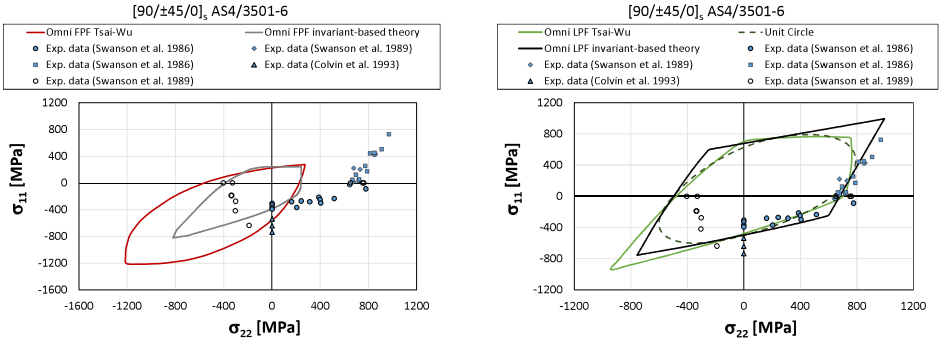

(a) Omni FPF envelopes. (b) Omni LPF envelopes and unit circle.

Fig. 13. σ_{22} - σ_{11} failure envelopes versus experimental results from the WWFE-I for a [90/±45/0]s AS4/3501-6 carbon/epoxy laminate.

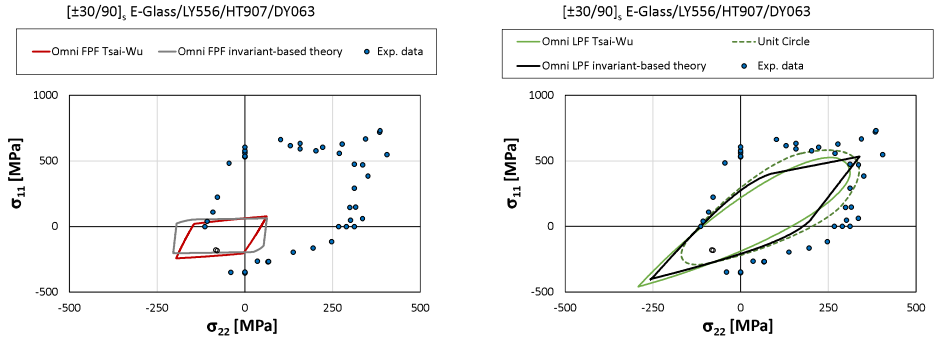

(a) Omni FPF envelopes. (b) Omni LPF envelopes and unit circle.

Fig. 14. σ_{22} - σ_{11} failure envelopes versus experimental results from the WWFE-I for a [±30/90]s E-glass/LY556/HT907/DY063 laminate.

CFRP laminates. As direct consequence of these remarks, the resulting unit circles for the same materials are no longer inscribed in the omni LPF envelopes, as represented in Fig. 17. Therefore, for the considered GFRPs, with a lower degree of anisotropy, the tensile and compressive strains-to-failure of a [0] coupon cannot be considered the only anchor properties to define omni failure analysis, and therefore the simplification of the unit circle does not apply to GFRPs.

Finally, it is noted that, as in the previous case (Fig. 13), the failure envelopes in Fig. 14 underpredict the experimental data in the compression–compression quadrant, which can be attributed to compression instability of the specimens under that loading condition.

The experimental results for a [±55]s E-glass/MY750/HY750/DY063 laminate are compared with the proposed omni LPF and unit circle envelopes in the σ_{22} - σ_{11} stress space, as illustrated in Fig. 18a. The conservatism of omni FPF envelopes is confirmed in this test case, as shown in Fig. 18b, while the predictive capability of omni LPF envelopes can be

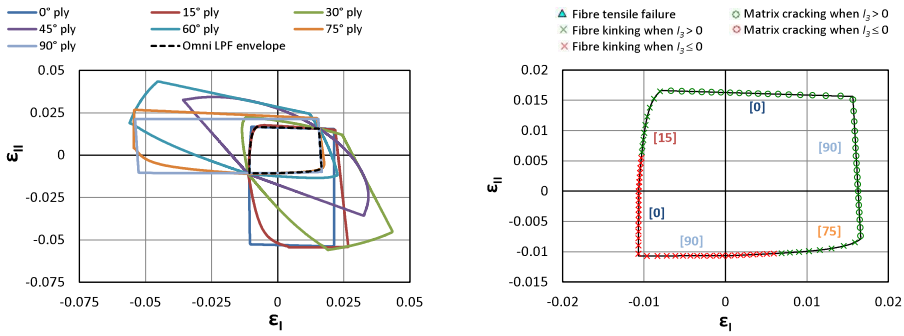

(a) Omni LPF envelope. (b) Controlling plies and failure modes.

Fig. 15. Omni strain LPF envelope, controlling plies and critical failure modes obtained with the 3D invariant-based failure criteria for E-glass/LY556/HT907/DY063.

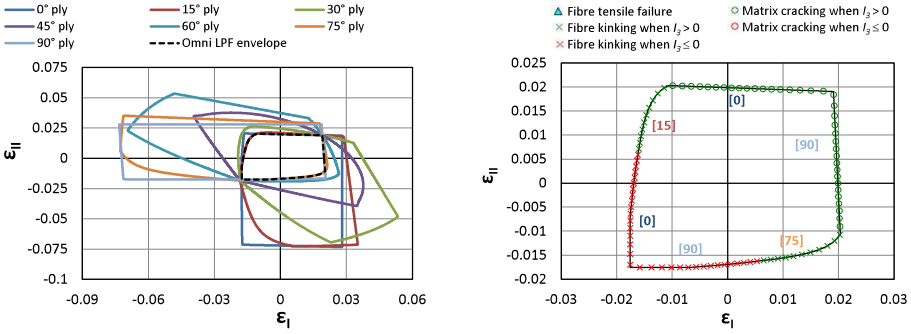

(a) Omni LPF envelope. (b) Controlling plies and failure modes.

Fig. 16. Omni strain LPF envelope, controlling plies and critical failure modes obtained with the 3D invariant-based failure criteria for E-glass/MY750/HY750/DY063.

acknowledged also in this study.

These 3 test cases provide clear indications on the huge benefits in using a LPF approach instead of FPF predictions. The larger domain when using LPF predictions allows to reduce conservatism in a remarkable way, without incurring on additional computational time. These benefits can be exploited immediately from the conceptual design stage of composite aerostructures, since the presented tool is invariant with respect to the laminate layup. The beneficial impact of this approach on the composites industry, where the consolidated practice in early design stage is to use FPF theories, such as Max strain or Tsai-Wu, can be significant.

A triaxial test case for laminate failure is also available from the WWFE-II. Due to the complexity of imposing a triaxial stress state with suitable load introduction systems, there is lack of reliable experimental results involving triaxiality. For UD laminates, such validation studies have been supported in the past by computational micromechanics; however, for multidirectional laminates, computational micromechanics is still not suitable for similar

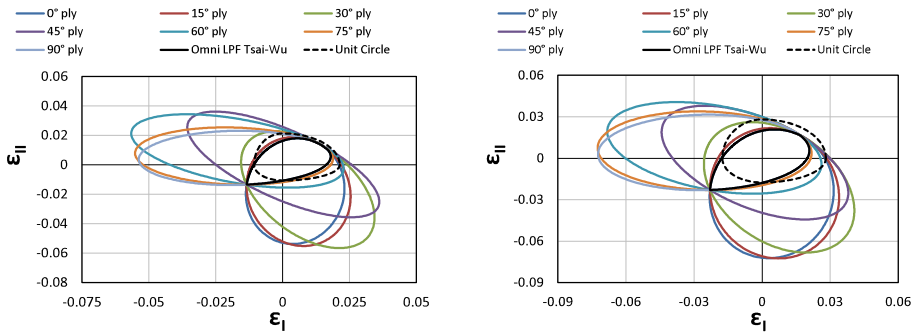

(a) E-glass/LY556/HT907/DY063. (b) E-glass/MY750/HY750/DY063.

Fig. 17. Omni LPF envelopes, based on Tsai-Wu, and unit circle envelopes in principal strain space for (a) E-glass/LY556/HT907/DY063 and (b) E-glass/MY750/HY750/DY063.

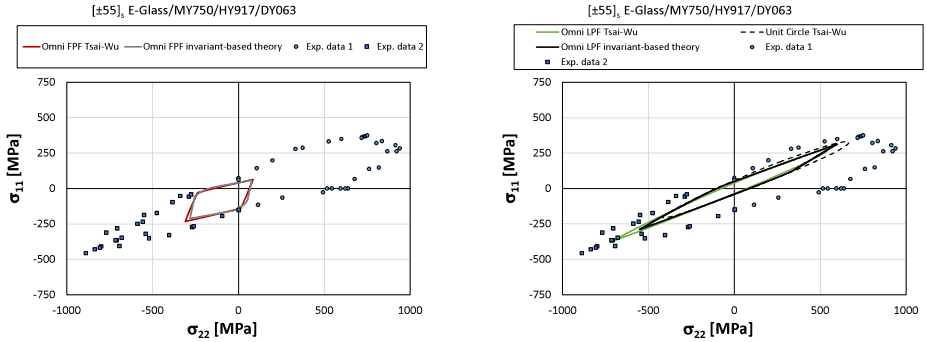

(a) Omni FPF envelopes. (b) Omni LPF envelopes and unit circle.

Fig. 18. σ_{22} - σ_{11} failure envelopes versus experimental results from the WWFE-I for a [±55]s E-glass/MY750/HY750/DY063 laminate.

studies due to the computational cost of running a micro-scale representative volume element of a multidirectional laminate. Herein, the aim is to assess the reliability of the proposed quick analytical approach to composite laminate failure, accepting a certain degree of conservatism. In the selected test case, glass/epoxy tubes were first subjected to an equal internal and external pressure, and then an axial compression load was incrementally applied up to failure, while keeping the pressure constant during the test[12]. The mechanical properties of E-glass/MY750/HY750/DY063 in the out-of-plane direction can be found in Ref.[12].

In order to predict the variation of the compressive strength σ_2 with through-thickness stress σ_3 (where σ_1=σ_3), a fully 3D omni LPF surface in stress space was generated for this material, to extract the envelope in the relevant section. To assess the conservatism of the proposed 3D omni LPF surface, a laminate failure envelope obtained superposing only ply failure envelopes of the relevant orientations (±35°) and the same failure model, was included in this study. Both surfaces and experimental data are shown in Fig. 19.

The predictions using the full 3D omni surface and the [±35°]s LPF surface in the relevant section are illustrated with a blue solid line and a dotted red line, respectively, and compared with experimental results in Fig. 20. This comparison shows that the laminate LPF envelope allows to reduce the conservatism of 3D omni LPF surfaces, with more accurate predictions, in the case of angle-ply laminates. However, in spite of providing conservative predictions, the omni LPF envelopes define, in a physically-based setting, a safe approach for laminate failure prediction that is independent of the particular lay-up sequence, thus making its application straightforward for any laminate of a given material system. It can, therefore, be used for preliminary design, analysis and optimization of composite structures without the need for recalculating the failure envelope. This allows simple generalization of ply-based criteria to laminate-based criteria, which is expected to contribute to significant time savings during the massive operations taking place, for instance, in multidisciplinary design optimization of composite aerostructures.

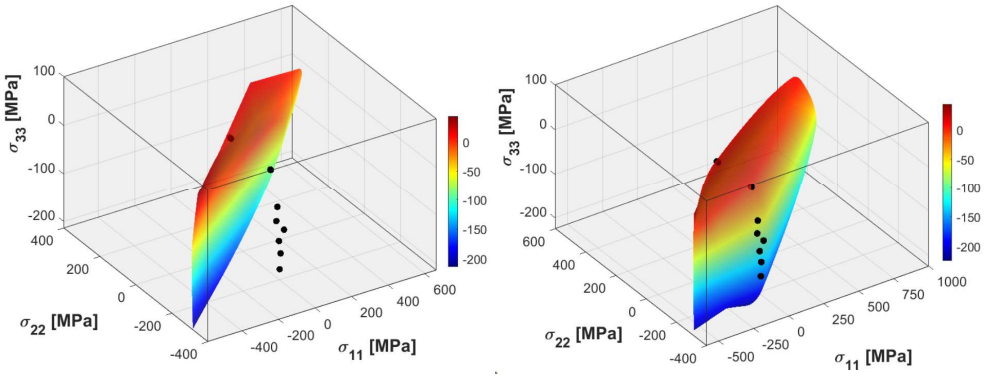

(a) 3D omni LPF surface. (b) 3D [±35]s LPF surface.

Fig. 19. 3D omni LPF (a) and [±35]s laminate LPF (b) surfaces versus experimental results from WWFE-II for a [±35]s E-glass/MY750 epoxy laminate.

Finally, in order to assess the importance of including the out-of-plane stresses in the failure analysis, the triaxial test case for a [±35]s E-glass/MY750 epoxy laminate from WWFE-II is again considered. In this case, the omni LPF envelopes assuming plane stress conditions are compared with the ones under general 3D stress states as shown in Fig. 21a. In Fig. 21b, the laminate LPF envelope is shown.

The omni LPF envelopes under plane stress provide similar predictions for both theories, as observed for the biaxial test cases from WWFE-I. When comparing these envelopes with the omni LPF surface, generated with the invariant-based theory, the design space is considerably reduced in the first and third quadrant, as a result of the effect of the out-of-plane stress. Although the available test data do not allow to assess with rigour how overestimated are the predictions of the plane stress models, the remarkable difference suggests that accounting for the effect of hydrostatic pressure can be very important in obtaining safe failure predictions for general laminates.

This becomes clear by analyzing the laminate LPF envelopes shown in Fig. 21b. The failure envelope from the [±35]s LPF surface confirms that the influence of the out-of-plane stress

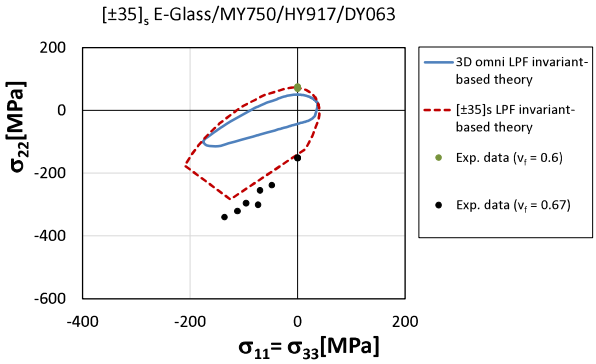

Fig. 20. σ_{22} - σ_{11}=σ_{33} failure envelopes versus experimental results from WWFE-II for a [±35]s E-glass/MY750 epoxy laminate. The experimental data is available for two different fibre volume fractions (v_f).

allows to capture the increase of strength under hydrostatic pressure and the reduced strength under triaxial tension/compression, and therefore, to get an improved correlation with the experimental data.

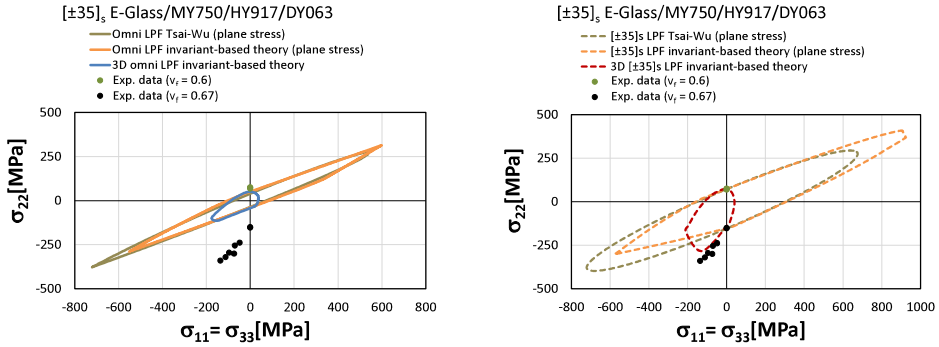

(a) Omni LPF predictions. (b) [±35]s LPF predictions.

Fig. 21. 3D omni LPF (a) and [±35]s laminate LPF (b) predictions under general stress states and plane stress conditions versus experimental results from WWFE-II for a [±35]s E-glass/MY750 epoxy laminate.

4.0 CONCLUSIONS

In the present work, an extension of a recently introduced concept, called omni strain failure envelope, is proposed by implementing a set of 3D phenomenological failure theories, known as the 3D invariant-based failure criteria, in order to address laminate failure under general 3D stress states and to identify critical failure modes. This concept allows simple generalization of ply-based criteria to laminate-based criteria, overcoming two important constraints in multidisciplinary design optimization of composite aerostructures: (i) computing time, by

establishing laminate failure criteria independently of ply discretisation, and (ii) excessive conservatism, by incorporating safe LPF criteria instead of overconservative FPF criteria.

A validation study of the predicting capability of omni LPF envelopes was performed using experimental results from the first and second WWFE. A good agreement was observed for the 2D cases, where the added value brought by the proposed envelopes was highlighted when analyzing glass-fiber composites, whose LPF is governed by different failure modes; LPF of CFRP laminates, on the other hand, is always governed by fibre failure.

Finally, a triaxial test case was studied. The proposed 3D omni LPF surface presented some degree of conservatism with respect to experimental data on an angle-ply laminate, providing, nevertheless, a safe design space with minimal analysis cost due to its laminate invariant character. However, this conservatism will not be observed in industry-standard CFRP quad laminates, containing [0], [±45] and [90] plies. Moreover, it is shown that the influence of the out-of-plane stress cannot be neglected to properly capture laminate failure under hydrostatic pressure and to obtain safe LPF predictions under general 3D stress states.

So, the described method proves to be a very robust tool, giving reliable and fast failure indications in either 2D or complex 3D stress states. Being a quick tool, it can be used for preliminary design and integrated in multidisciplinary design optimization platforms, meeting the industrial need for computational efficiency, while simplifying the failure analysis and sizing of composite laminates.

ACKNOWLEDGEMENTS

This work was supported by the OptiMACS project, which is funded by the European Union's Horizon 2020 research and innovation programme under the Marie Skłodowska-Curie grant agreement n° 764650.

REFERENCES

1. D. Gay, S. V. Hoa, and S. W. Tsai. *Composite materials: Design and applications*. 2014.
2. J. Echaabi, F. Trochu, and R. Gauvin. Review of failure criteria of fibrous composite materials. *Polymer Composites*, 17(6):786–798, 1996.
3. F. Paris and K. E Jackson. A Study of Failure Criteria of Fibrous Composite Materials. *NASA Scientific and Technical Information (STI) Program Office*, (March):76, 2001.
4. A. Puck and W. Schneider. On failure mechanisms and failure criteria of filament-wound glass-fibre/resin composites. *Plastics and Polymers*, 37:33–43, 01 1969.
5. A. Puck and H. Schürmann. Failure analysis of FRP laminates by means of physically based phenomenological models. *Failure Criteria in Fibre-Reinforced-Polymer Composites*, 3538(96):832–876, 1998.
6. C. G. Dávila, P. P. Camanho, and C. A. Rose. Failure Criteria for FRP Laminates. *Journal of Composite Materials*, 39(4):323–345, 2005.
7. S. T. Pinho, C. G. Dávila, P. P. Camanho, L. Iannucci, and P. Robinson. Failure Models and Criteria for FRP Under In-Plane or Three-Dimensional Stress States Including Shear Non-linearity. *Nasa/Tm-2005-213530*, (February):68, 2005.
8. G. Catalanotti, P. P. Camanho, and A. T. Marques. Three-dimensional failure criteria for fiber-reinforced laminates. *Composite Structures*, 95:63–79, 2013.

9. P. P. Camanho, A. Arteiro, A. R. Melro, G. Catalanotti, and M. Vogler. Three-dimensional invariant-based failure criteria for fibre-reinforced composites. *International Journal of Solids and Structures*, 55:92–107, 2015.
10. M. Vogler, G. Ernst, and R. Rolfes. Invariant based transversely-isotropic material and failure model for fiber-reinforced polymers. *Computers, Materials and Continua*, 16(1):25–49, 2010.
11. P. P. Camanho, A. Arteiro, G. Catalanotti, A. R. Melro, and M. Vogler. Three-dimensional invariant-based failure criteria for transversely isotropic fibre-reinforced composites. In *Numerical Modelling of Failure in Advanced Composite Materials*, pages 111–150. Woodhead Publishing, Cambridge, 2015.
12. M. J. Hinton and A. S. Kaddour. Triaxial test results for fibre-reinforced composites: The Second World-Wide Failure Exercise benchmark data. *Journal of Composite Materials*, 47(6-7):653–678, 2013.
13. H. Thom. A review of the biaxial strength of fibre-reinforced plastics. *Composites Part A: Applied Science and Manufacturing*, 29(8):869–886, 1998.
14. A. Arteiro, G. Catalanotti, J. Reinoso, P. Linde, and P. P. Camanho. Simulation of the Mechanical Response of Thin-Ply Composites: From Computational Micro-Mechanics to Structural Analysis. *Archives of Computational Methods in Engineering*, 26(5):1445–1487, 2019.
15. A. Catapano and M. Montemurro. On the correlation between stiffness and strength properties of anisotropic laminates. *Mechanics of Advanced Materials and Structures*, 26(8):651–660, 2019.
16. S. W. Tsai and J. D. D. Melo. An invariant-based theory of composites. *Composites Science and Technology*, 100:237–243, 2014.
17. S. W. Tsai and J. D. D. Melo. A unit circle failure criterion for carbon fiber reinforced polymer composites. *Composites Science and Technology*, 123:71–78, 2016.
18. B. Vermes, S. W. Tsai, A. Riccio, F. Di Caprio, and S. Roy. Application of the Tsai's modulus and double-double concepts to the definition of a new affordable design approach for composite laminates. *Composite Structures*, (October):113246, 2020.
19. M. J. Hinton, A. S. Kaddour, and P. D. Soden. *Failure Criteria in Fibre Reinforced Polymer Composites: The World-Wide Failure Exercise*. 2004.
20. A. S. Kaddour and M. J. Hinton. Maturity of 3D failure criteria for fibre-reinforced composites: Comparison between theories and experiments: Part B of WWFE-II. *Journal of Composite Materials*, 47(6-7):925–966, 2013.